Modern trends in selecting and designing Pelton turbines

By F. de Siervo and A. Lugaresi
Chief* and Senior Engineer*

This article presents the results of an extensive statistical investigation made on more than 90 Pelton turbines manufactured all over the world and completes a research on conventional hydraulic turbines of which the first part on Francis and the second part on Kaplan were published respectively in the August 1976 and December 1977 issues of this journal[1, 2].

IN THE FOLLOWING, several considerations that are common to Pelton, Kaplan and Francis turbines are omitted for simplicity; the authors suggest that a better understanding of the present subject will be achieved by making reference to the previous articles on Francis and Kaplan machines mentioned above.

Emphasis is given to multi-jet, vertical-type Pelton turbines because of their prevalence in high capacity applications; horizontal machines are considered only for specific speed and main wheel dimensions.

The collected data show a trend towards the use of machines with capacities of 300 MW, or more, and with wheel diameters up to about 5.5 m.

The research covers, with some exceptions, the period between 1960 and 1977.

Table I gives the main features of the installations investigated as taken from the references, while the diagrams are based on the project data and dimensions collected by an extensive enquiry as was made for Kaplan turbines.

The curves were drawn by the simple regression procedure adopted in the previous studies.

General selection criteria

The same characteristic constant used for Francis and Kaplan turbines is adopted for the Pelton turbines:

$$n_s = n P_t^{0.5} H_n^{-1.25} \qquad (1)$$

where P_t is the rated capacity of the turbine.

The Pelton impulse turbine differs considerably from the Francis and Kaplan reaction turbines considered in the previous articles, being a partial-admission machine in which the hydraulic energy is transmitted to the wheel by a discrete number of nozzles independent from each other. Consequently the main hydrodynamic characteristics of the turbine has to be referred to one jet only. The specific speed n_{sj} relevant to one jet is then introduced:

$$n_{sj} = n (P_t/i)^{0.5} H_n^{-1.25} \qquad (2)$$

and the statistical relationship

$$n_{sj} = n_{sj}(H_n) \qquad (3)$$

is sought between the one-jet specific speed and the design head.

The available data have been divided into two groups, depending on the year of design of the turbines.

This gives the two regression curves indicated on the left-hand side of Fig. 1, which are described as follows:

1960-1964 $\quad n_{sj} = 78.63\ H_n^{-0.243}$

1965-1977 $\quad n_{sj} = 85.49\ H_n^{-0.243}$

The correlation coefficients and the standard deviations are respectively:

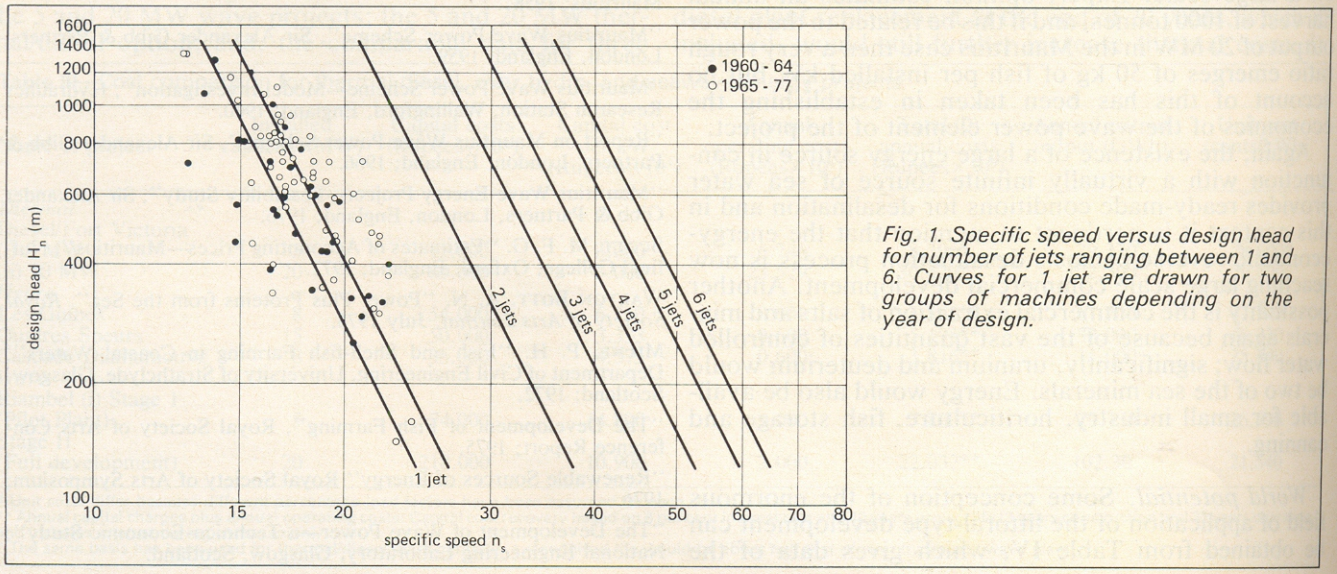

Fig. 1. Specific speed versus design head for number of jets ranging between 1 and 6. Curves for 1 jet are drawn for two groups of machines depending on the year of design.

*Hydromechanical Department Electroconsult, 20151 Milan, Italy

Notations*

D_2 = Wheel pitch diameter (m)
D_j = Jet diameter (m)
H_n = Turbine net design head (m)
K_u = Runner peripheral velocity coefficient
H_s = Distance between wheel centreline and maximum water level within the casing (m)
n = Turbine rotation frequency (rev/min)
n_f = Turbine runaway rotation frequency (rev/min)
n_s = Turbine specific speed
n_{sj} = Turbine specific speed per jet
i = Number of jets
η = Turbine efficiency (p.u.)
ϕ = Jet effeciency (p.u.)
P_t = Turbine rated capacity (kW)
Q = Turbine rated flow (m^3/s)
v = Water velocity at spiral case inlet (m/s)
r = Statistical curve correlation coefficient
s = Statistical curve standard deviation
g = Gravitational acceleration (m/s^2)

(*) For notations relevant to the machine main dimensions refer to the relevant figures.

$r=-0.50$ $s=2.75$

$r=-0.70$ $s=1.65$

These show a high degree of grouping of the data related to the chosen interpolating function. The trend to increase the n_{sj} value for a given head is evident between the two periods indicated.

Contrary to the procedure adopted for the studies on Francis and Kaplan turbines, it was not possible to split the data relevant to the period 1965-1977 into two different groups, because no significant trend towards a higher n_{sj} was evident. This is mainly because Pelton turbines are hydraulically simpler than reaction turbines and their design, in the last ten years, has probably come closer to the optimum than for Francis and Kaplan.

It is worth mentioning that a conspicuous reduction of the overall dimensions of Pelton turbines has been achieved recently by increasing the number of nozzles following thorough investigations into the related mechanical problems and on the interactions between the jets. In fact the percentages of 5 and 6 nozzle turbines out of the total number considered are .25 and .46 respectively for the two periods of time indicated.

The right-hand side of Fig. 1 shows the n_s values as a function of H_n for turbines with up to 6 nozzles. By comparing the n_s given in Fig. 1 for the 6 nozzle turbines with the n_s relevant to Francis machines for the same period, one sees that in the overlapping area (H_n ranging between 200 and 600) the specific speed is clearly lower for Pelton while the slope is higher.

The lower n_s values are a consequence of the partial admission of the machine. Investigations have been made with the aim of increasing the specific speed, n_s, of Pelton turbines further; the solution proposed envisages installing two wheels on the same vertical shaft with nozzles fed by only one spiral distributor[3,4].

Fig. 2 compares the $n_{sj}=n_{sj}(H_n)$ curve of Fig. 1 of the period 1965-1977 with similar curves taken from the references[5,6,7]. Curves 2 and 3 of Fig. 2 show, in the field of low heads, n_{sj} values higher than those given by the

Table I—Pelton turbines at major hydro schemes

Powerplant	Manufacturer	Year	Head (m)	Capacity (MW)	Rotation frequency (rev/min)
Anpogawa I	Fuji	1959	342.16	12.2	514
Aricota II	Fuji	1965	311.8	12.2	514
Askara	Kvaerner Brug	1967	655	73.53	500
Aurland	Kvaerner Brug	1969	840	242.65	375
Ausserfragant I-II	Vöest-Alpine	1964	485	28.97	500
Ausserfragant III	Vöest-Alpine	1976	485	36.76	500
Banbajima	Fuji	1961	319	22.2	450
Batiaz	Charmilles		626	80.319	428.6
Bavona	Escher Wyss	1962	886	70.2	428.6
Bitsch	Charmilles		737	105.1	375
Bjolvefossen	Kvaerner Brug	1969	835	36.76	600
Bluhbach III	Voith	1971	145	1.87	375
Borgund	Kvaerner Brug	1971	850	91.91	500
Chivor	Riva Calzoni	1972	803.5	134.3	450
Combe d'Avrieux	Neyrpic	1972	857	131.25	500
De Sabla	BLH Vöest-Alpine	1960	450	18.6	450
Diessbach II	Vöest-Alpine	1968	703	12.5	750
El Colegio II	Voith	1967	945	57.7	514
El Toro	Charmilles		557	121.2	333
Etzel	Escher Wyss	1969	473	43	500
Evanger	Kvaerner Brug	1965	790	110.29	500
Fionnay	Charmilles		870	56.78	428.6
Fisher	Fuji	1968	610	46	500
Foothill	Escher Wyss	1969	161.50	10.88	327.3
Grosio III	Franco Tosi	1963	600	107.1	333
Grytten	Kvaerner Brug	1971	920	143.38	500
Guadalupe	Hitachi	1964	554	52.7	450
Guatape	Escher Wyss	1965	836	78.2	514.3
Idikki	Neyrpic	1969	660	134.4	375
Jnnerfragant	Escher Wyss	1966	1177	32.9	750
Jurún Marinalá	Vevey	1967	652.5	23.38	800
Kaonertal	Voith	1961	890	78.75	500
Kodayar I	Vevey	1965	948	66.18	500
Kops	Voith	1965	780	85.3	500
Kundah II	Domionion	1959	713.24	36.76	428.5
Kundah III	Dominion	1975	411.49	63.23	333.3
Kurobegawa IV	Fuji	1058	580	86.5	360
Kurobegawa IV	Hitachi	1973	580	89.5	360
Kuttiadi	Fuji	1965	662	27.6	600
Lago Delio	Ansaldo-F. Tosi	1967	731.65	126.8	500
Lago Delio	Riva Calzoni	1967	731.99	127.32	500
Lang-Sima	Kvaerner Brug	1975	1126	257.35	428
Lete-Sava	Riva Calzoni	1962	647.14	55.15	500
Loon Lake	Hitachi	1968	345.3	85.8	200
Lotru	Neyrpic	1968	788	187.5	375
Malta	Voith	1973	1030	181.2	500
Mantaro	Ansaldo R. Calzoni	1968	850	123.5	450
Mauranger	Charmilles		825	127	500
Mayrhofen	Voith	1965	470	63.1	375
McCloud Pit (1)	BLH Vöest-Alpine	1963	340	76.47	240
Middlefork	Voith	1963	559	61.15	400
Miyagawa III	Fuji	1960	477.179	12.5	720
Moccasin	Hitachi	1968	368.5	53.3	300
Mont-Cenis (2)	Neyrpic	1963	869	200	375
Moncenisio	Riva Calzoni	1962	1304	125	428
Motosu	Fuji	1956	453	12.6	720
Nacazaki	Fuji	1957	253	10.8	400
Nam Phrom	Fuji	1970	373	21	429
Naturns	Voith	1960	1129	60.81	500
Nendaz	Charmilles		1004	67.6	500
New Colgate	Voith	1966	413	167	180
Okuyama	Fuji	1961	336	10.5	600
Paute	Hydroart	1977	667	116	360
Peruana del Santa	BLH Vöest-Alpine	1963	398	31.6	450
Poatina	Fuji	1974	829.06	60.1	600
Ralston	Voith	1963	382	79.1	240
Rio Lindo	Hitachi	1970	405	24.418	450
Santa Isabel	Voith	1969	840	18.4	750
S. Fiorano I	Ansaldo-F. Tosi	1967	1403.8	140	500
S. Fiorano II	Ansaldo-F. Tosi	1969	1401.4	139.66	600
Sellrain Silz	Escher Wyss	1976	1233.06	241.9	500
Siso II	Kvaerner Brug	1968	645	91.91	500
Skjomen	Kvaerner Brug	1969	585	102.94	428
Steg	Charmilles		622	55.4	500
Sy-Sima	Kvaerner Brug	1974	885	314.71	300
Tabuaco	Neyrpic	1960	451	35.74	500
Tapanti	Vevey	1969	450	35.29	450
Timpagrande	Franco Tosi	1972	538.04	67.5	500
Tochio	Fuji	1956	292	16	400
Tonaru	Mitsubishi	1965	596.42	27.1	600
Tysso II	Escher Wyss	1964	720	97	500
Uvdal I	Kvaerner Brug	1964	565	47.06	500
Vadheim I	Vöest-Alpine	1959	300	2.21	300
Vadheim II	Vöest-Alpine	1970	300	6.03	500
Vernayaz	Charmilles		610	21	500
Veytaux	Vevey	1968	877	63.97	600
Voldertal II	Vöest-Alpine	1965	650	3.46	1000
Wadagawa II	Fuji	1958	470	61.4	300
Wurten IV	Vöest-Alpine	1967	485	29.89	500
Wurten V	Vöest-Alpine	1976	485	36.76	500
Ylja	Kvaerner Brug	1971	670	64.71	600

(1) BLH Design
(2) In collaboration with Alsthom-Charmilles

curve derived by the authors, even though they are relevant to older machines. The references listed in Fig. 2 do not indicate the characteristics of the machines on which curves 2 and 3 are based, thus hampering the comparison with curve 1 which refers mainly to vertical shaft, multi-jet turbines.

As for Francis and Kaplan turbines, the curves given in Fig. 1 should be taken with some degree of caution, adapting the value of n_s to the particular characteristics of the installations. Economic considerations lead to the choice of the highest possible n_s value, for a given head which corresponds to a six-nozzle turbine, to minimize dimensions and costs of both electro-mechanical equipment and civil works. On the other hand limitations to this choice may be imposed by mechanical design factors such as the maximum allowable peripheral velocity of the generator rotor or the minimum feasible sizing of the Pelton turbine. This is particularly evident in the field of high head machines for which these considerations are binding for high and low capacities, respectively.

Once the value of n_s is decided from Fig. 1, the best rotation frequency is determined by Eq. (1); the rated frequency of the turbine will coincide with one of the synchronous frequencies nearest to the ideal one. For large, low-head turbines the trend will be to choose the higher frequency to reduce dimensions and costs while for high-head machines the choice may be influenced by the same design consideration as stated before.

The selected synchronous frequency will then determine the actual n_{sj} value to be used for operating on the subsequent diagrams.

Another highly characteristic constant is commonly used for Pelton turbines, ie the ratio D_j/D_2 of the jet diameter to the wheel pitch diameter.

Propositions developed later in this article show that this constant virtually determines the main geometrical characteristics of the machine. D_j/D_2 is strictly related to the specific speed per jet, n_{sj}. This can be easily demonstrated by introducing the following relationships:

- peripheral velocity coefficient:

$$k_u=\pi D_2 n/[60\sqrt{(2gH_n)}] \quad \ldots (5)$$

- capacity equation:

$$P_t=9.81\eta H_n Q=9.81\eta H_n i(\pi D_j/4)\phi\sqrt{(2gH_n)}. \quad \ldots (6)$$

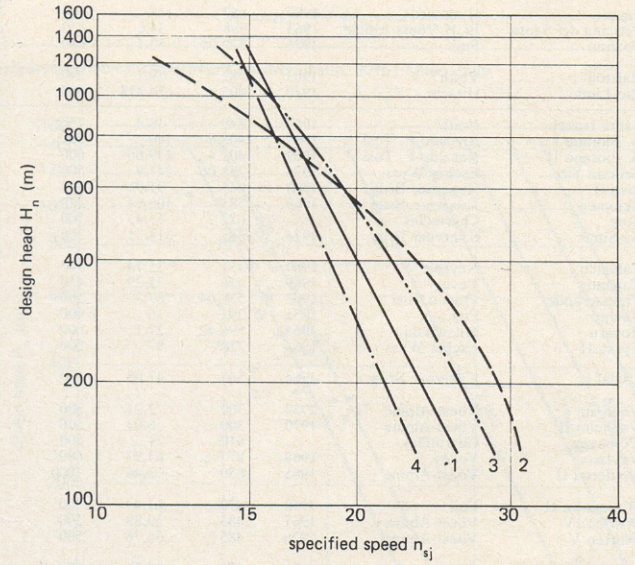

Fig. 2. Specific speed versus design head from different sources. Curve 1 is derived from Fig. 1; curve 2 is taken from reference 7; curve 3 is taken from reference 5; and curve 4 is taken from reference 6.

where ϕ represents the jet efficiency defined as the ratio of the actual water velocity to the spouting velocity.

By substituting Eqs. (5) and (6) in Eq. (2) one obtains:

$$n_{sj}=494.2K_u(D_j/D_2)\sqrt{(\eta\phi)} \quad \ldots (7)$$

and, assuming the values of 0.89 and 0.976 for η and ϕ respectively, which are considered representative of a broad field of real cases, one obtains:

$$n_{sj}=460.6K_u(D_j/D_2) \quad \ldots (8)$$

Considering the limited variations of K_u that will be detailed later on, the relationship between n_{sj} and D_j/D_2 is evident.

The elevation of the turbine above the tailrace water level is determined by the necessity to avoid any interference between the wheel and the agitated water surface within the turbine casing, during both steady state operation and during transients. The parameter H_s is then introduced, being the distance between the wheel centreline and the maximum water level within the casing in steady conditions.

According to the literature[8,9], the value of H_s depends basically on the total turbine discharge Q, and increases with it. On the other hand the data examined show that for a given discharge Q, the value of this increases with the net head H_n of the machine. Probably this phenomenon can be ascribed to the ventilation effect which is stronger for high head turbines because of their higher frequency of rotation, other conditions being equal. Considering the preceding, the best correlation from the examined data has been found by plotting the H_s values versus the ratio of Q to n_s, as indicated in Fig. 3.

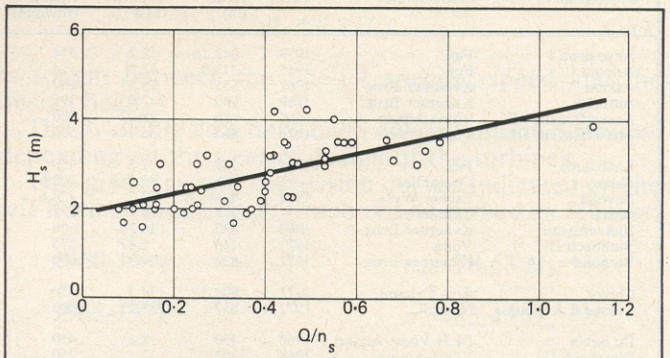

Fig. 3. Clearance between wheel and centreline and casing water level.

The interpolating function is:

$$H_s=1.87+2.24Q/n_s \quad \ldots (9)$$

where

$$r=0.67, \text{ and } s=0.52$$

The considerable scattering of the data shown by Fig. 3 is related to several factors, among which the most important are:

- turbine installation levels imposed by the owner;
- water level variations during transients, particularly in case of long tailrace channels; and,
- different solutions for the aeration of the casing.

The runaway coefficient n_f/n, the ratio of the runaway rotation frequency to the rated one, which is necessary to define the design of the electric generator, is expressed as a function of n_{sj} in Fig. 4. No interpolating function is indicated because of the very high scattering of the data collected. Different choices of the independent variable

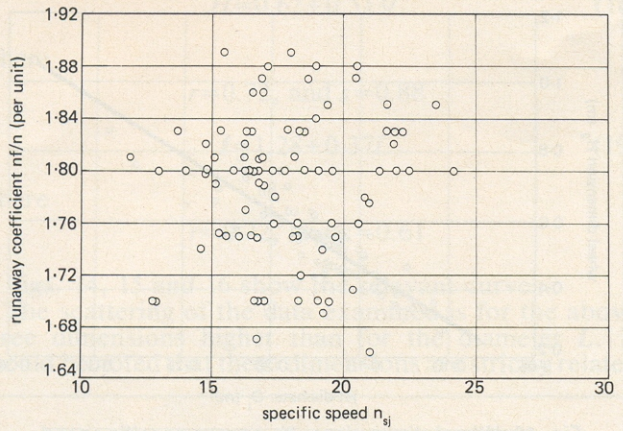

Fig. 4. Ratio between runaway and rated frequency of rotation versus specific speed.

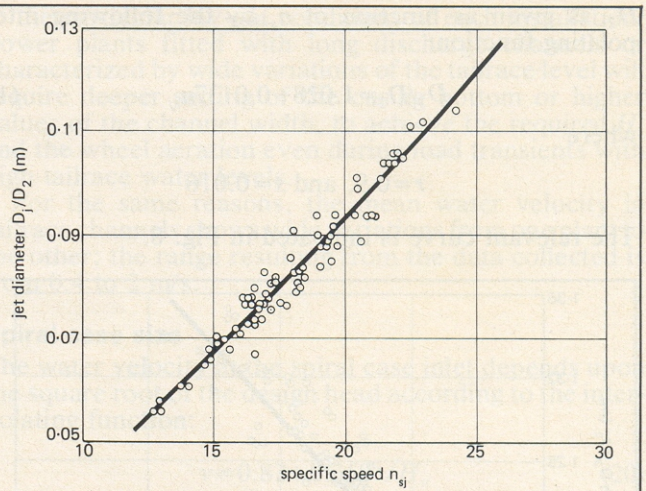

Fig. 6. Ratio between jet and wheel pitch diameter versus specific speed.

have been checked with no improvement to the results. The most likely origin of this scattering must be attributed to the considerable variation of the runaway rotation frequency with the number of jets in operation. Head variations and ventilation effects amplify the dispersion. Fig. 4 shows that more than 50 per cent of the data examined are confined within the range 1.76 to 1.84, which can be considered satisfactory for preliminary estimation.

Wheel dimensions

The runner's main dimensions are determined by the peripheral velocity coefficient K_u already defined in Eq. (5).

The function $K_u=K_u(n_{sj})$, calculated by correlating the available data, is

$$K_u=0.5445-0.0039n_{sj} \quad \ldots \quad (10)$$

with

$$r=-0.63, \text{ and } s=0.009$$

The corresponding curve is indicated in Fig. 5.

The scattering of the data examined for the interpolating curve is mainly because of the different hydraulic design of the bucket adopted by the various manufacturers and the total number of buckets selected for each single case.

Once the value of K_u and the frequency of rotation n are established, it is possible to calculate the value of D_2 from Eq. (5). D_2 can also be calculated using the parameter D_j/D_2.

Fig. 6 shows the curve $D_j/D_2=(D_j/D_2(n_{sj})$ whose interpolating equation is:

$$D_j/D_2=n_{sj}/(250.74-1.796n_{sj}) \quad (11)$$

where

$$r=0.97, \text{ and } s=0.003$$

Adopting suitable values of η and ϕ in Eq. (6), the jet diameter D_j is found; D_2 is then determined introducing D_j in Eq. (11). Assuming the values already indicated for η and ϕ in determining Eq. (8), D_2 will show the same value derived through the peripheral velocity coefficient. The other wheel dimensions indicated in Fig. 7 may then be obtained.

The outer wheel diameter D_3, referred to the diameter

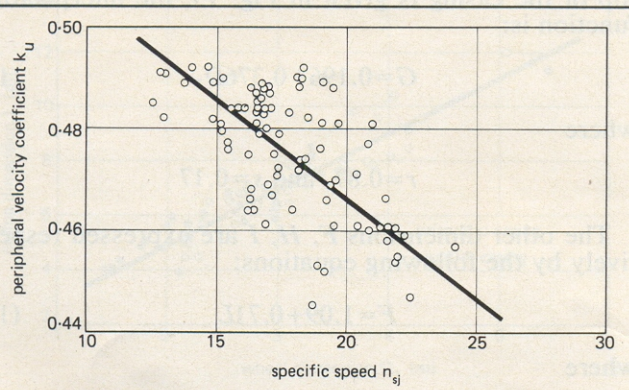

Fig. 5. Peripheral velocity coefficient versus specific speed.

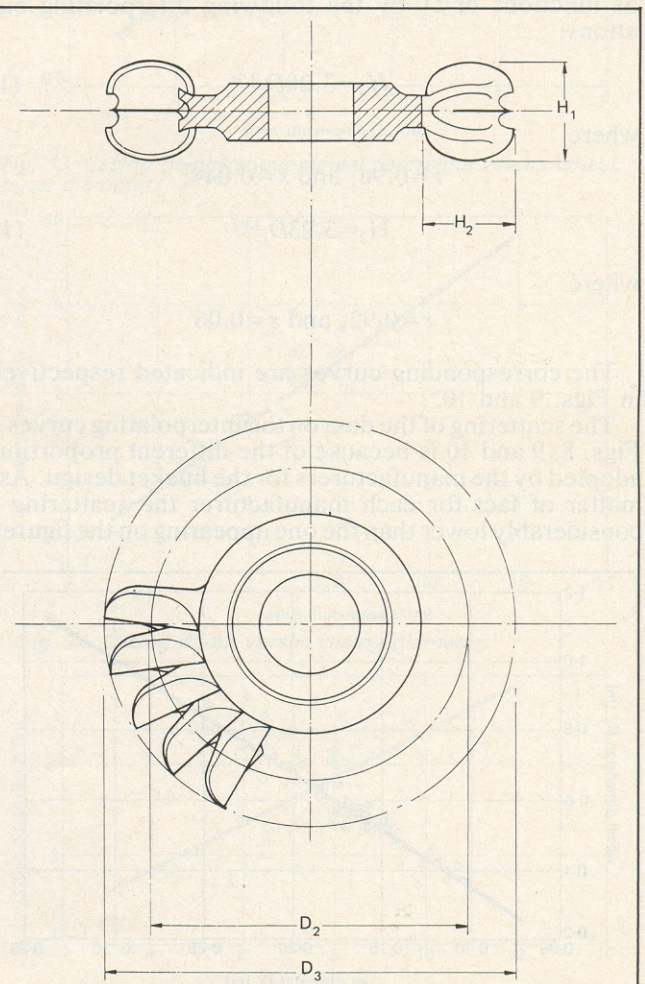

Fig. 7. Wheel dimensions; their values are indicated in Fig. 6. and Figs. 8 to 10.

D_2, is given as function of n_s by the following interpolating function:

$$D_3/D_2=1.028+0.0137n_{sj} \quad (12)$$

where

$$r=0.9, \text{ and } s=0.016$$

The relevant curve is indicated in Fig. 8.

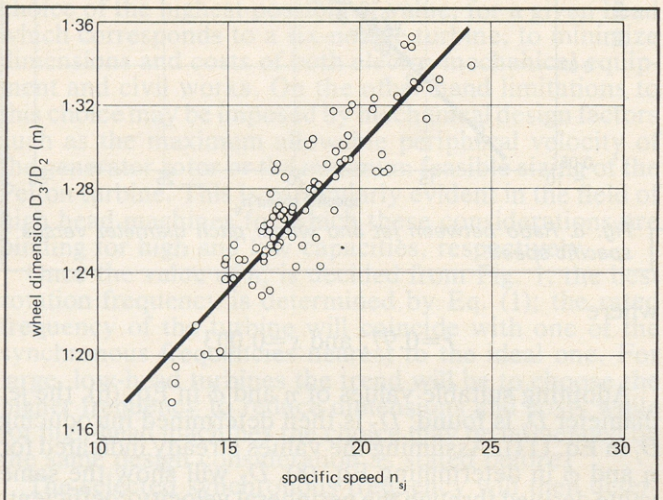

Fig. 8. Wheel dimensions, D_3/D_2, versus specific speed.

The width and the length of the wheel bucket are given as functions of D_j by the following interpolating equations:

$$H_1=3.20D_j^{0.96} \quad (13)$$

where

$$r=0.96, \text{ and } s=0.044,$$

$$H_2=3.23D_j^{1.02} \quad (14)$$

where

$$r=0.92, \text{ and } s=0.06$$

The corresponding curves are indicated respectively in Figs. 9 and 10.

The scattering of the data on the interpolating curves in Figs. 8, 9 and 10 is because of the different proportions adopted by the manufacturers for the bucket design. As a matter of fact for each manufacturer the scattering is considerably lower than the one appearing on the figures.

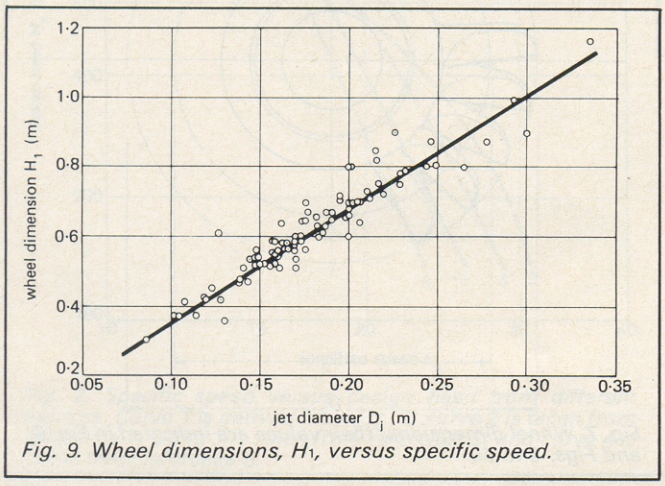

Fig. 9. Wheel dimensions, H_1, versus specific speed.

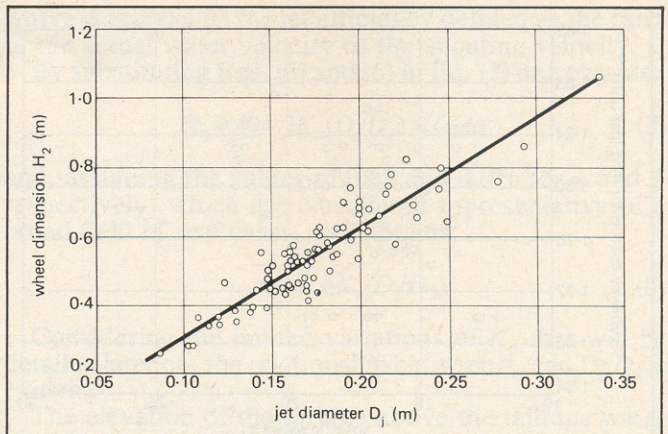

Fig. 10. Wheel dimensions, H_2, versus specific speed.

Combining Eqs. (1), (4), (5), (10) with the capacity equation (6), it is possible to write Q as a function of D_3 and H_n in the following way:

$$Q=(D_3)^2F(H_n)i$$

The function $F(H_n)$, within the n_s values considered, ranged between 0.36 and 0.34 with a variation of only 6 per cent.

It is therefore possible to conclude from these statistical diagrams that, as a first approximation, the water flow of a Pelton turbine depends only on the square of the outer wheel diameter and on the number of jets. This consideration is similar to the one indicated for Kaplan turbines[2].

Casing dimensions

The dimensions of the Pelton turbine casing depend essentially on the outer diameter D_3 of the wheel.

The casing dimensions considered are indicated in Fig. 11.

The most expressive of them is the diameter L which gives the plan size of the casing; for prismatic casings this value has been assumed equal to the average diameter of the circles inscribed and circumscribed on the casing, as indicated in Fig. 11.

The interpolating function for the diameter L is:

$$L=0.78+2.06D_3 \quad (15)$$

where

$$r=0.92, \text{ and } s=0.66$$

The relevant curve is indicated in Fig. 12.

The distance G between the wheel centreline and the top of the casing is given in Fig. 13; the interpolating function is:

$$G=0.196+0.376D_3 \quad (16)$$

where

$$r=0.87, \text{ and } s=0.17$$

The other dimensions F, H, I are expressed respectively by the following equations:

$$F=1.09+0.71L \quad (17)$$

where

$$r=0.81, \text{ and } s=0.89$$

$$H=0.62+0.513L \quad (18)$$

where

$$r=0.72, \text{ and } s=0.88$$

$$I=1.28+0.37L \quad (19)$$

where

$$r=0.72, \text{ and } s=0.61$$

Figs. 14, 15 and 16 show the relevant curves.

The scattering of the data examined is for the above three dimensions higher than for the diameter L. It should be noted that these dimensions are strictly related to the particular lay-out conditions of each installation. Power plants fitted with long discharge channels or characterized by wide variations of the tailrace level will require deeper setting of the casing bottom or higher values of the channel width, to achieve the required H_s and the wheel aeration even during load transients with high tailrace water levels.

For the same reasons, the mean water velocity in tailrace channels shows wide variations from one plant to the other; the range resulting from the data collected is from 0.4 to 2 m/s.

Spiral case size

The water velocity at the spiral case inlet depends upon the square root of the design head according to the interpolating function:

$$v=0.82+0.358\sqrt{H_n} \quad (20)$$

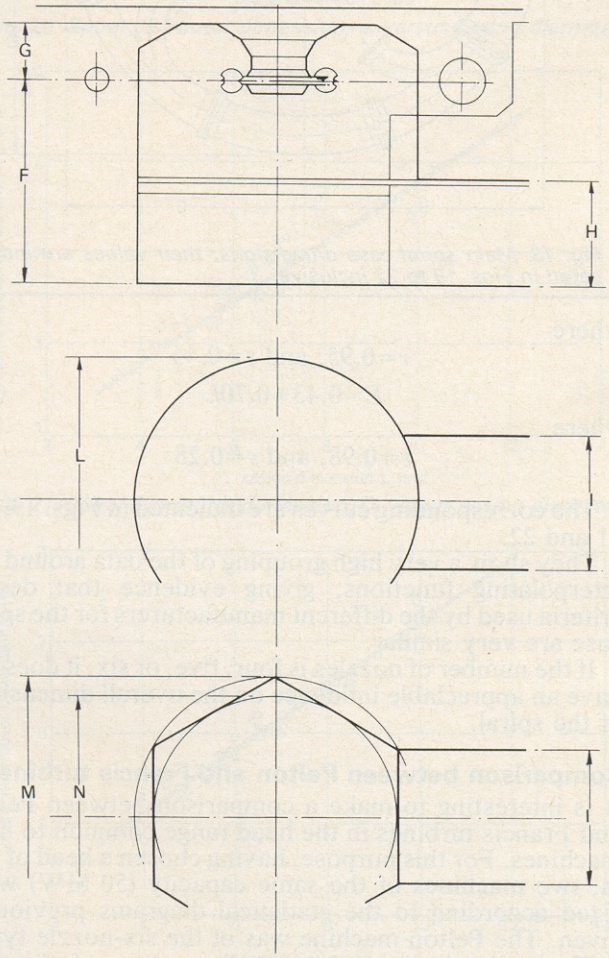

Fig. 11. Casing dimensions; their values are indicated in Figs. 12 to 16 inclusive.

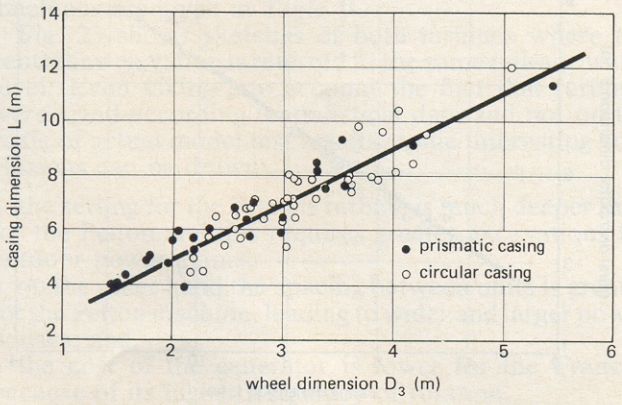

Fig. 12. Casing diameter versus wheel outer diameter.

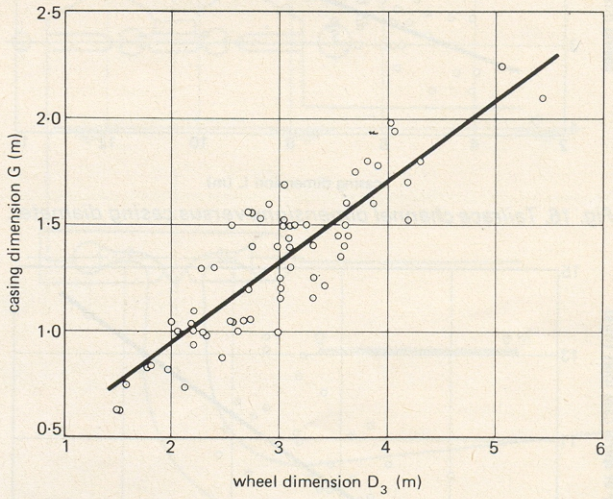

Fig. 13. Casing height above wheel centreline versus wheel outer diameter.

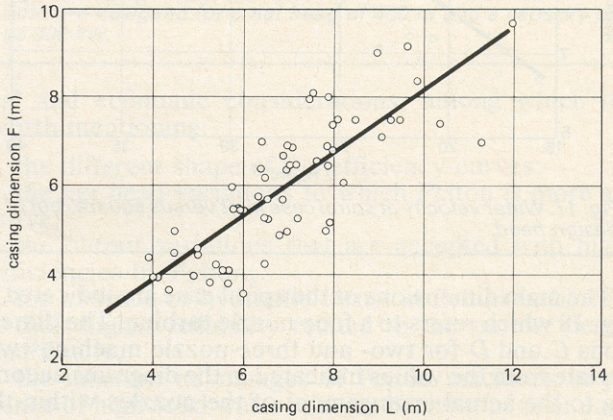

Fig. 14. Casing depth versus casing diameter.

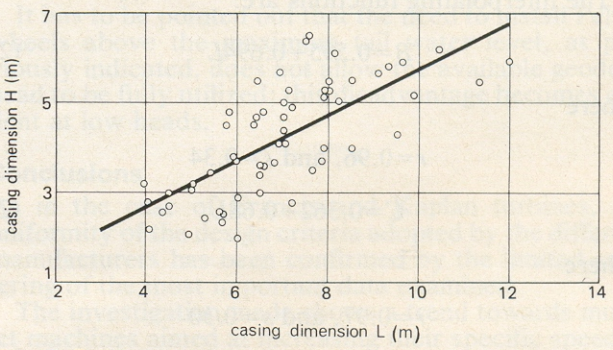

Fig. 15. Tailrace channel dimensions versus casing diameter.

where

$$r=0.74, \text{ and } s=1.42$$

The corresponding curve is indicated in Fig. 17.

The head losses of the spiral case, calculated according to Eq. (20) and referred to the rated head, increase approximately with the cubic root of H_n. For high head plants the influence of the spiral case head losses becomes negligible in comparison with the head losses of the whole hydraulic system; this allows an increase in v and consequently a reduction in the spiral inlet diameter without compromising the overall system efficiency.

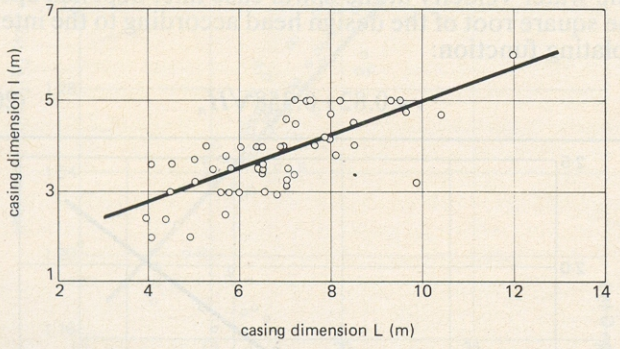

Fig. 16. Tailrace channel dimensions versus casing diameter.

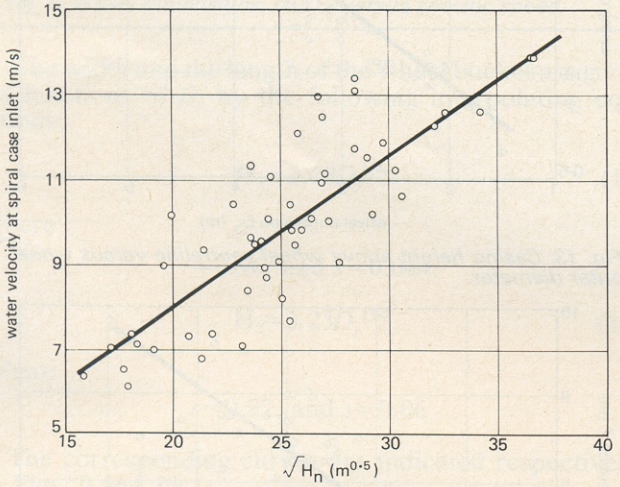

Fig. 17. Water velocity at spiral case inlet versus square root of design head.

The main dimensions of the spiral case are indicated in Fig. 18 which refers to a four-nozzle turbine. The dimensions C and D for two- and three-nozzle machines will deviate from the values indicated in the diagrams according to the actual arrangement of the nozzles within the turbine casing.

The interpolating functions are:

$$B=0.595+0.694L \tag{21}$$

where

$$r=0.96, \text{ and } s=0.34$$

$$C=0.362+0.68L \tag{22}$$

where

$$r=0.97, \text{ and } s=0.30$$

$$D=-0.219+0.70L \tag{23}$$

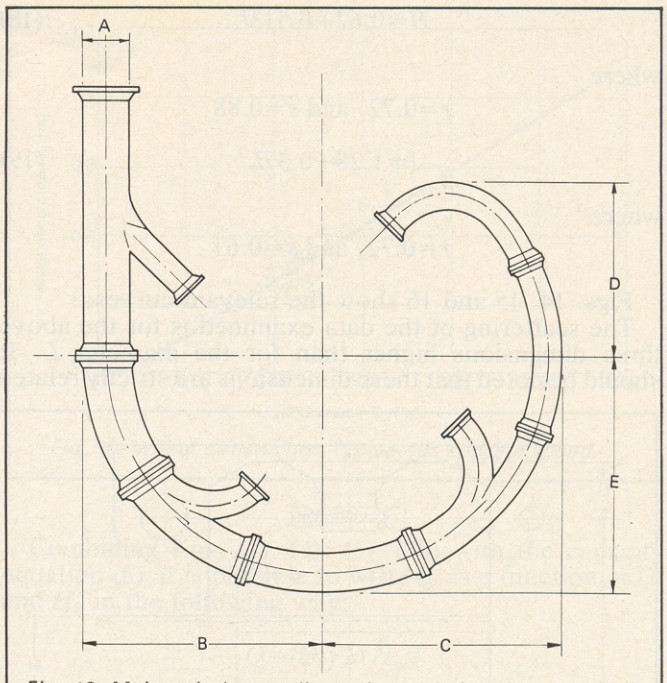

Fig. 18. Main spiral case dimensions; their values are indicated in Figs. 19 to 22 inclusive.

where

$$r=0.95, \text{ and } s=0.44$$

$$E=0.43+0.70L \tag{24}$$

where

$$r=0.98, \text{ and } s=0.28$$

The corresponding curves are indicated in Figs. 19, 20, 21 and 22.

They show a very high grouping of the data around the interpolating functions, giving evidence that design criteria used by the different manufacturers for the spiral case are very similar.

If the number of nozzles is four, five, or six, it does not have an appreciable influence on the overall dimensions of the spiral.

Comparison between Pelton and Francis turbines

It is interesting to make a comparison between Pelton and Francis turbines in the head range common to both machines. For this purpose, having chosen a head of 400 m, two machines of the same capacity (50 MW) were sized according to the statistical diagrams previously given. The Pelton machine was of the six-nozzle type.

The main design data and dimensions of the two

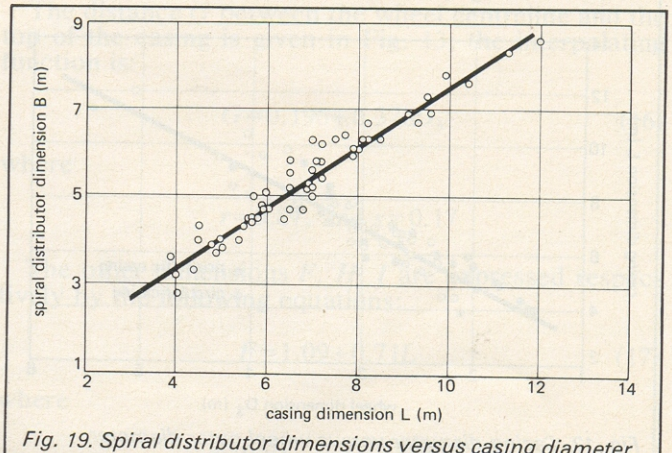

Fig. 19. Spiral distributor dimensions versus casing diameter.

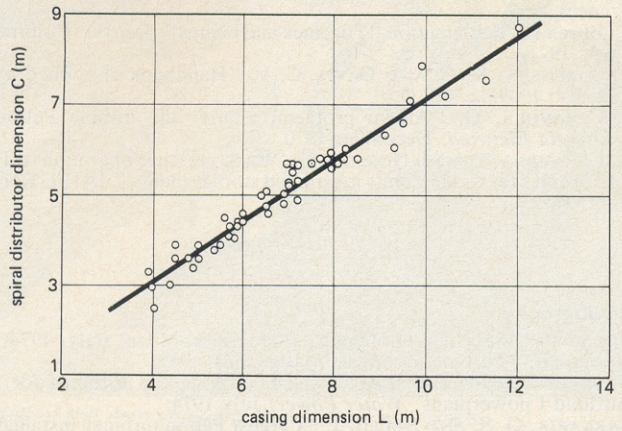

Fig. 20. Spiral distrbutor dimension, c, versus casing diameter.

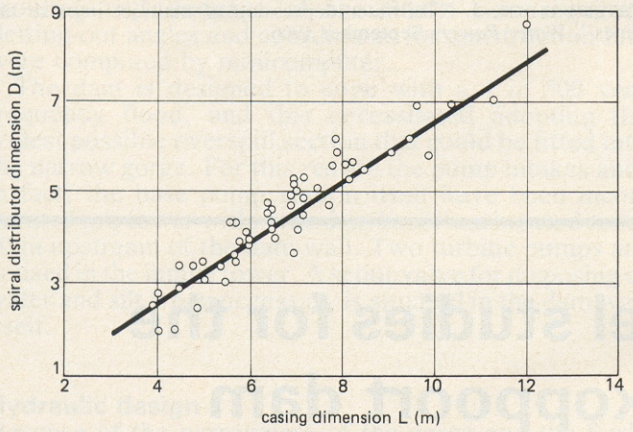

Fig. 21. Spiral distributor dimension, D, versus casing diameter.

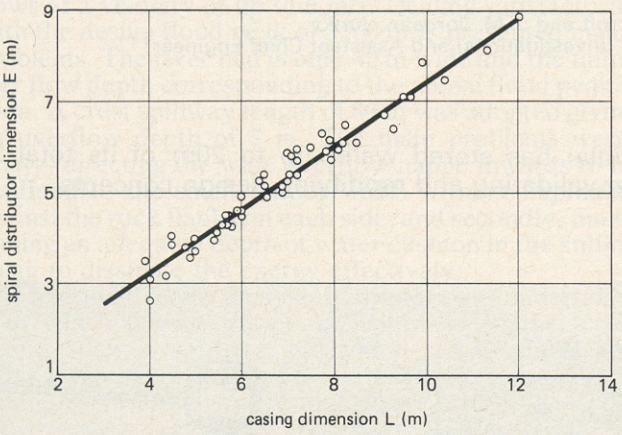

Fig. 22. Spiral distributor dimension, E, versus casing diameter.

machines are given in Table II.

Fig. 23 shows sketches of both turbines where the centreline elevation is referred to the same tailrace water level. Even taking into account the fact that turbines were sized according to statistical data and not on the basis of actual model test results, some interesting conclusions can be drawn:

- the setting for the Francis turbine is much deeper than for the Pelton and this requires greater excavations for outdoor power plants;
- on the other hand the spacing between units is greater for the Pelton machine, leading to wider and larger power houses; and,
- the cost of the generator is lower for the Francis, because of its higher frequency of rotation.

The actual choice depends upon several other technical and economic considerations, among which it is worth mentioning:

- the different shape of the efficiency curves;
- the net head variations to which Pelton is more sensitive;
- the output variations that are accepted with higher efficiencies by Pelton;
- the absence of hydraulic thrust in Pelton turbines;
- their higher reliability related to the simpler design; and finally,
- the inherent advantages of Pelton machines in presence of high solid water content because of their easier and less expensive maintenance.

It has to be pointed out that the need to install Pelton wheels above the maximum tail water level, as previously indicated, does not allow the available geodetic head to be fully utilized; this disadvantage becomes evident at low heads.

Table II—Comparison of Pelton (P) and Francis (F) turbines for the same head and rating

	P	F
H_n (m)	400	400
P (kW)	50 000	50 000
n_s	46.9	75
n (rev/min)	375	600
D_3 (m)	2.74	1.40
D_2 (m)	2.12	1.42
D_j (m)	0.187	
A (m)	1.51	1.33
E+D (m)	9.15	5.56
N (m)		5.96
S (m)		11.00
L (m)	6.40	
F (m)	5.60	
H (m)	3.90	
H_s (m)	2.55	−3.30

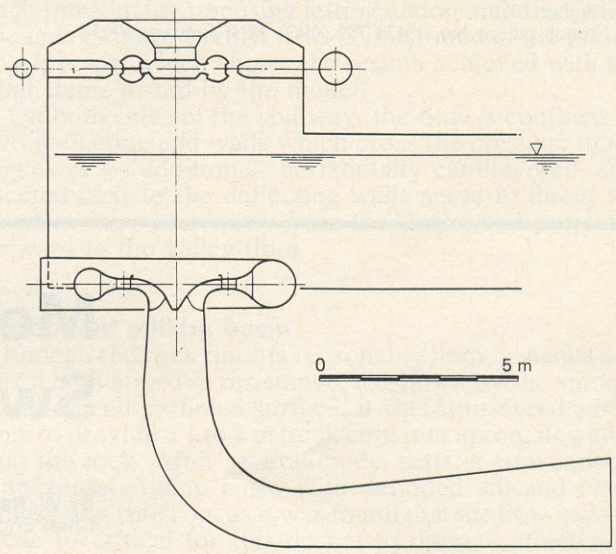

Fig. 23. Comparison between Pelton and Francis turbines. Both are designed for a net head of 400 m and a capacity of 50 000 kW.

Conclusions

As in the case of Francis and Kaplan turbines, the uniformity of the design criteria adopted by the different manufacturers has been confirmed by the limited scattering of the most important data examined.

The investigation made shows a trend towards multijet machines aimed at increasing their specific speed to minimize dimensions and costs.

Partial compensation of tailrace level fluctuations pressurizing the casing and further increase of the specific speed at low heads by the adoption of two wheels on the same vertical shaft are presently being considered by manufacturers to extend the range of utilization of Pelton turbines. □

Acknowledgements

The authors wish to thank all the manufacturers indicated in Table 1 for their valuable contribution in supplying the main design data and dimensions of their machines that made possible the present study.

References

1. De Siervo, F. and de Leva, F. "Modern trends in selecting and designing Francis turbines", *Water Power and Dam Construction;* August 1976.
2. de Siervo, F. and de Leva, F. "Modern trends in selecting and designing Kaplan turbines", *Water Power and Dam Construction;* December 1977 and January 1978.
3. Chuzhin, G. V. and Edel, Yu. U. "Increasing the running speed of impulse hydraulic turbines", *Gidroteknicheskoe Stroitel'stvo;* November 1970.
4. French patent No. 1.431.789, class F03; January 1965.
5. Vivier, L. "Turbines hydrauliques" (Editions Albin), Paris, France; 1966.
6. Bureau of Reclamation "Turbines and pumps", Denver, Colorado, USA, 1971.
7. Sorensen, K. E. and Davis, C. V. "Handbook of applied hydraulics"; 1969.
8. Ceravola, O. "Alcuni problemi relativi alle turbine Pelton", *L'Energia Elettrica;* December 1970.
9. Ceravola, O. and Noseda, G. "Back pressure operation of Pelton turbines for ternary units in pumped storage plants", IAHR, Rome, Italy; 1972.

Bibliography

Coen, M. "Macchine idrauliche" (Signorelli); Milan, Italy, 1974.
Rubbo, B. "Turbine idrauliche" (Bignami); 1967.
Brekke, H. and Hofseth, B. "243 MW Pelton turbines for the Aurlund I powerplant" *Water Power;* July 1974.
Sarkaria, G. S. and Sallo, J. "Largest Pelton turbines installed in New Colgate powerplant, California" *Energy International;* January 1971.
Osterwalder, J. "Tailwater depression of multi-jet impulse turbines", *Water Power;* September 1966.

Model studies for the Swakoppoort dam

By W. Ravenscroft and J. M. Jordaan, Junior
Chief Engineer (Investigations) and Assistant Chief Engineer*

Swakoppoort arch dam, in South West Africa (Namibia) has stored water up to 20m of its total 35m depth. Hydraulic model studies were highly effective in validating and modifying design concepts.

Swakoppoort was built to augment the existing borehole and surface water schemes supplying water to the central area of South West Africa—mainly Windhoek, the capital city. Situated in a narrow gorge in the Swakop river, some 55 km downstream of the Von Bach dam, the new structure impounds 70×10^6 m^3. Up to 10×10^6 m^3 per annum of untreated water from Swakoppoort will be pumped via a 600 mm steel pipeline 51 km in length to the purification works at Von Bach dam and from there to Windhoek and other bulk water consumers. Extension of the water purification plant and an additional 1100 mm concrete jacketed prestressed steel cylinder pipeline 62 km in length from the Von Bach dam purification works to Windhoek, form part of the total scheme.

The design and construction of the double curvature arch dam itself was undertaken by the South West Africa Branch of the Department of Water Affairs. A computer program based on the trial load method of analysis was used in the design. Geological investigations were carried out by the Geological Survey Division of the Department of Mines.

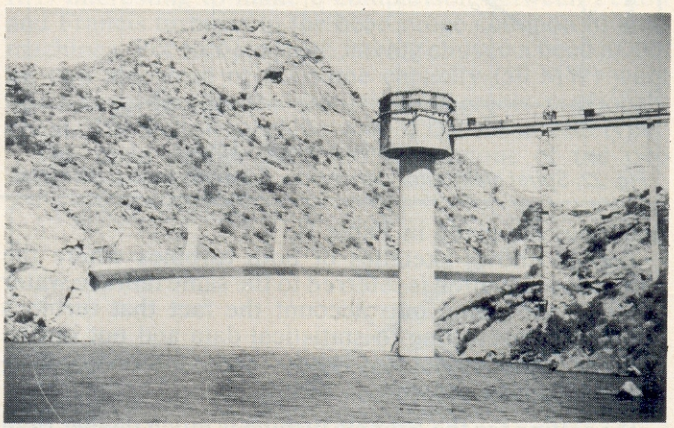

Upstream view of the dam and outlet tower.

At the dam site fine to medium grained granites occur in the river section and lower flanks, and medium- to coarse-grained granites and pegmatites in the upper levels, which created some problems in accurately blasting to specified excavation lines.

Pronounced jointing and open fissures confined the siting of the dam to within fairly narrow limits. Curtain

* Department of Water Affairs, Kaiser Street, Windhoek, South West Africa.